Journal of Materials Chemistry A

Accepted Manuscript

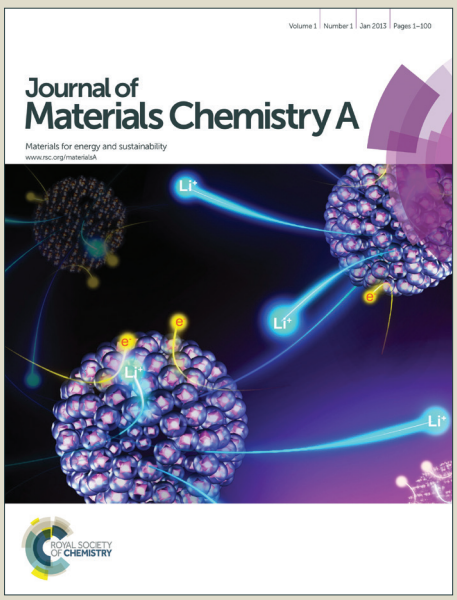

ROYAL SOCIETY OF CHEMISTRY

www.rsc.org/materialsA

Ag size-dependent visible-light-responsive photoactivity of Ag-TiO_2 nanostructure based on surface plasmon resonance

Zhuo Jiang, Qin Ouyang, Bosi Peng , Youxiang Zhang, and Ling Zan*

College of Chemistry and Molecular Science, Wuhan University, Wuhan 430072, P. R. China.
E-mail: irlab@whu.edu.cn(L. Zan) Tel: 86 27 6875 2919

Anatase TiO_2 nanocrystals with regular polyhedron morphology and co-exposed {001} and {101} facets are prepared, and then ultrafine Ag nanoparticles (SAg NPs) with different sizes are loaded on those TiO_2 facets (denoted as SAg-TiO_2) through a novel in situ photoreduction approach. For comparison, Ag nanoparticles (PAg NPs) are also loaded on TiO_2 facets (denoted as PAg-TiO_2) by a traditional photodeposition method. The experimental results show PAg NPs with size of ~20 nm only appeared on the {101} facets of TiO_2, while SAg NPs with much smaller size (1-6 nm) highly dispersed on both {001} and {101} facets of TiO_2. The size of Ag NPs plays an important role on surface plasmon resonance (SPR) effect and the photogenerated carrier separation process, and those Ag NPs loaded on TiO_2 facets show size-dependent photoactivity for the RhB degradation. SAg-TiO_2 with ultrafine SAg NPs on both {001} and {101} facets of TiO_2 result in more substantial visible-light-responsive photoactivity and stability than PAg-TiO_2 with larger Ag NPs on {101} facets of TiO_2. Moreover, the RhB photodegradation reaction rate constant of SAg-TiO_2 with Ag particle size of ~1 nm is 10 and 21.3 times higher than that of PAg-TiO_2 and the pristine TiO_2, respectively.
Keywords: Ag nanoparticles; in-situ photoreduction; size-dependent photoactivity; surface plasmon resonance effect.

Over the past decades, semiconductor photocatalysis has attracted increasing attention as a most promising technology for wastewater remediation,[1,2] solar energy conversion,[3] and hydrogen energy production.[4] Among various semiconductor materials, anatase titania (TiO_2) has been regarded as one of the most important photocatalysts due to its physical and chemical stability, low cost, and high UV-light-responsive photoactivity.[5] Nevertheless, TiO_2 displayed ineffective visible light utilization and low quantum yields, which impaired its applications to great aspect.[6-13] To solve these problems, several strategies such as metal nanoparticles (NPs) loading,[6-9] metal ion[10,11] or nonmetal ion[12,13] doping have been proposed to expand the spectral responsive range of TiO_2. Especially, some noble metal NPs with surface plasmon resonance (SPR) effect are loaded on broad bandgap semiconductor (TiO_2, $BiVO_4$) to obtain visible-light-driven photoactivity.[6,14] For example, $BiVO_4$ loaded with Ag, Au, Pt or Pd NPs exhibited visible-light-deriven photoactivity.[6] Also, photocurrent was increased 1.7 times when Ag clusters are deposited on TiO_2 nanosheet.[14]

Among those noble metal NPs loaded, Ag NPs are most widely used in the field of photocatalysis due to its low price and strong SPR absorption though its catalytic effect is weaker than Au or Pt NPs. Therefore, various methods such as photodeposition, deposition–precipitation, impregnation and sol–gel process, have been developed to prepare Ag NPs loaded on TiO_2.[14-17] For example, Ag NPs with size in the range of 20~160 nm were loaded on TiO_2 nanosheet film electrode through a photodeposition process,[14] while Ag NPs with relatively uniform size (~20 nm) was loaded on TiO_2 under UVA irradiation for 20 min.[15] Moreover, Ag NPs derived from deposition–precipitation process can be increased from ~10 nm to ~16 nm with enhancing the Ag loading amount from 4.0wt% to 1.5wt%.[16] Mohamed et al.[17] also prepared Ag NPs with size of ~15 nm loaded on TiO_2-SiO_2 through an impregnation process. Generally, the above preparation routes generated Ag NPs with size greater than 15 nm and/or their aggregation. Those large Ag NPs may also consume the photogenerated holes in addition to the SPR effect during the irridiation, and results in a low photoactivity because it was reported that the energetic property of the loaded Ag NPs may approach to that of bulk Ag upon enhancing its size gradually, which makes the Ag sites become recombination center of the photogenerated carriers.[18] Therefore, it is still a challenge to develop an effective approach for controlling the size of Ag NPs loaded on TiO_2.

Herein, anatase TiO_2 nanocrystals with regular polyhedron morphology and co-exposed {001} and {101} facets are prepared according to the previous method,[19] and then an in situ photoreduction approach is used to synthesis ultrafine Ag NPs with different sizes loaded on those TiO_2 facets (denoted as SAg-TiO_2) by adjusting the photoreduction condition. Moreover, Ag NPs are also loaded on TiO_2 facets (denoted as PAg-TiO_2) by a traditional photodeposition method for comparison. It is found that the two deposition methods lead to different Ag NPs sizes and distributions on TiO_2 facets, and those Ag NPs loaded on TiO_2 facets show size-dependent photoactivity for the RhB degradation. The ultrafine SAg NPs loaded on both {001} and {101} facets of TiO_2 result in much higher visible-light-responsive photoactivity than the PAg NPs with larger size only on the {101} facets of TiO_2. The corresponding mechanisms of Ag NPs growth and its size-dependent photoactivity are also investigated based on the characterization results of the surface plasmon resonance (SPR) effect and the photogenerated carrier separation process.

RESULTS AND DISCUSSION

Fig. 1 shows the TEM and SEM images of the obtained TiO_2 nanocrystals and its Ag-loaded products (PAg-TiO_2 and SAg-TiO_2) derived from different processes. As can be seen from Fig. 1A, those anatase TiO_2 nanocrystals show regular polyhedron morphology with co-exposed {001} and {101} facets although its size distribution is in the range of 30-70 nm, and the percentage of

{001} facets can be calculated to be ~40% according to the previous report.[20] Those Ag NPs derived from different preparation processes show different particle sizes, distributions and morphologies on the TiO_2 facets. For instance, PAg-TiO_2 mainly contains spherical Ag NPs with size of ~20 nm only appeared on the exposed {101} facets of TiO_2(Fig. 1B), while SAg-TiO_2 shows ultrafine Ag NPs with much smaller size (~1 nm) are highly dispersed on both {001} and {101} facets (Fig. 1C). Furthermore, the HRTEM image (Insert of Fig. 1D) of PAg-TiO_2 shows the clear lattice fringes with lattice spacing of 0.235 and 0.204 nm, corresponding to the (111) and (200) facets of cubic Ag. Similarly, the HRTEM image (Insert of Fig. 1E) of SAg-TiO_2 shows the (111) atomic plane with lattice spacing of 0.235 nm is identical to the theoretic value of Ag crystal. The above results indicate that those particles loaded on TiO_2 facets are metallic Ag microcrystals.

The above different sizes and distributions of Ag NPs on TiO_2 facets might be related to their respective loading process as shown in Scheme 1. According to the previous literature,[6] the traditional photodeposition process by using $AgNO_3$ solution as precursor would only lead to the reduction of those Ag^+ ions adsorbed on {101} facets of TiO_2 because the photogenerated electrons of TiO_2 move to {101} facets during UV light irradiation.[6] Moreover, Ag NPs would continue to grow on {101} facets and form bigger size upon prolonging the light irradiated time because Ag is a good electron sink,[16-18] and therefore, PAg-TiO_2 mainly contains Ag NPs with large size only appeared on the exposed {101} facets of TiO_2 as shown in Scheme 1A, which is also consistent with the previous reports.[16-18,21,22] However, during the preparation of SAg-TiO_2, the formed $AgIO_3$ as Ag source can uniformly coat on all facets of TiO_2 polyhedron nanocrystals, and then ultrafine Ag NPs with high dispersity are formed on both {001} and {101} facets owing to the limited shift ability of the loaded solid state $AgIO_3$ particles, which also retard the Ag particles' growth during the decomposition into metallic Ag NPs under the following UV light irradiation as shown in Scheme 1B.

Moreover, it was found that the particle size of Ag NPs on both {001} and {101} facets of TiO_2 can be adjusted by controlling the photoreaction temperature and UV light wavelengths as shown in Fig. S1, and the corresponding size change trends of SAg NPs upon the photoreaction condition are summarized in Fig. 1D. As can be seen from Fig. 1D and S1, the photoreaction temperature plays a key role in the size of SAg NPs. When the photoreaction temperature is increased from 0°C to 10°C, SAg NPs size changed from 2.4 nm to 1 nm, and then increased from 1 nm to 6 nm once the temperature is enhanced from 10°C to 20°C. For most chemical reactions, elevated temperatures can accelerate the reaction rate. When the temperature increase, $AgIO_3$ decomposes rapidly, the size of Ag NPs will be large. So we need to control a suitable temperature to get ultrafine Ag NPs. Similarly, UV light wavelength is also an influencing factor of the SAg NPs size.

When the wavelength was changed from 254 nm to 365 nm, SAg NPs decreased from 5 nm to 1 nm, which is highly dispersed on the facets of TiO_2. Due to the light-decomposition of $AgIO_3$, different UV irradiation wavelengths bring different external energy, then affecting the size of Ag. Just as the short UV wave length (254 nm) has a higher energy, so the size of SAg NPs increased. For convenience, the samples of SAg-TiO_2 with different Ag NP sizes are named SAg-TiO_2 (x nm), where x nm means the Ag NPs size loaded on TiO_2 facets. For example, SAg-TiO_2 (1 nm) means the minimal size (~1 nm) of Ag NPs loaded on TiO_2 facets, which can be obtained by 365 nm UV light irradiation at 10°C as shown in Fig 1C and S1B.

To make clear the SAg growth mechanism during the photoreaction process, the transformation from $AgIO_3$-TiO_2 to Ag-TiO_2 was observed by DRS spectra shown in Fig. S2. It can be observed that the visible light absorbance increased with prolonging UV irradiation time in the first 30 min and then decreased. It indicates that the formed $AgIO_3$ can be photolysized completely in the initial 30 min, after that the decrease of visible light absorption can be attributed to the transformation of Ag NPs to AgO_x. To confirm the transformation, we also use XPS to detect the sample after irradiating by UV light for 1h. One peak corresponding to AgO (367.4 eV) was observed in the XPS spectra of SAg-TiO_2 (Fig S3A),[16] indicating that the irradiation time is a dominant influencing factor on the photoreduction process. The crystalline structure and phase characteristics of SAg-TiO_2 (1 nm) and $AgIO_3$-TiO_2 can be obtained by XRD patterns shown in Fig. S4A. Both samples display a highly crystalline, and all strong diffraction peaks of $AgIO_3$-TiO_2 can be readily indexed to the tetragonal TiO_2 (JCPDS No: 65-5714) and orthorhombic $AgIO_3$ (JCPDS No: 45-0880), respectively. Due to the light-sensitive property of $AgIO_3$, no XRD peak of $AgIO_3$ can be detected after the UV irradiation. The anatase TiO_2 before and after the UV irradiation shows the same diffraction patterns in intensity ratios, indicating that UV irradiation does not cause any significant change in the crystal structure of TiO_2. XPS spectrum (Fig. S4B) of SAg-TiO_2 (1 nm) derived from UV light (365 nm) irradiation for 30 min shows two characteristic peaks of Ag at binding energies of 368.4 eV and 374.27 eV, which can be ascribable to $Ag3d_{5/2}$ and $Ag3d_{3/2}$ spin-orbital splitting photoelectrons, respectively. And in Fig.S3B , no peak corresponding to I 3d was observed in the XPS spectra of SAg-TiO_2 (1 nm). The above binding energies confirm that the deposited silver is of metallic nature.[14,23]

UV-Vis diffuse reflectance spectra (DRS) of TiO_2 nanocrystals and its Ag NPs loaded products (PAg-TiO_2 and SAg-TiO_2) are shown in Fig. 2. An intense visible absorption band in the range of 400-800 nm appears for all Ag NPs loaded products, which can be primarily ascribed to the typical surface plasmon resonance (SPR) absorption of Ag NPs. Moreover, the visible light absorption intensity increases upon decreasing the Ag NPs size, and SAg-TiO_2 (1 nm) with 1 nm

Ag NPs loaded on TiO_2 facets possesses the highest visible light absorption among those Ag NPs loaded products. It can be confirmed by roughly estimating the Abs at 490 nm, which is changed from 0.75 to 0.40 when the Ag particle size decrease from 20 nm to 1 nm. Namely, the SPR effect of Ag NPs loaded on TiO_2 facets is sensitive to the particle size, which is consistent with the previous results.[24,25] Therefore, it can be concluded that SAg-TiO_2 (1 nm) should have the best photocatalytic activity under visible light irradiation due to its high SPR effect among those Ag NPs loaded on products.

Photoluminescence (PL) spectra can be used to understand the fate of the photogenerated electron–hole pairs in semiconductor under irradiation. Fig. 3A shows the PL spectra of TiO_2, SAg-TiO_2 and PAg-TiO_2 in the range of 370-550 nm. The main emission peak at 468 nm is related to the bandgap (2.65 eV) of the anatase TiO_2.[26,27] As can be seen from the histogram of the PL emission peak intensities at 468 nm listed in Fig. 3A, the PL intensity of the pure TiO_2 is significantly higher than that of Ag-TiO_2, indicating Ag NPs loading could influence the recombination process of the photogenerated carriers in TiO_2. Moreover, the PL intensity of different Ag-TiO_2 samples revealed the effect of Ag NPs size on the carrier recombination, and a lower PL intensity means a lower carrier recombination rate.[28] Therefore, it can be concluded that the ultrafine SAg NPs (1-5 nm) can greatly promote the photogenerated carrier separation in the SAg-TiO_2 because their relative low PL intensity as shown in Fig. 3A. Once SAg NPs grow to 6 nm, the PL intensity at 468 nm exhibits more obvious increase, which is similar to the previous reports on Au, Pt NPs.[29-32] The reason can be ascribed to the following facts: The electrons excited from the ultrafine SAg NPs can quickly migrate to the TiO_2 under visible-light irradiation, which can prevent the carrier recombination, and the smaller the Ag NPs, the faster the electron transfer, which then results in lower carrier recombination rate. When Ag NPs grow to 6 nm, it may become charge recombination centers, and result in the PL intensity increase.[18,31] Time-resolved PL spectra shown in Fig. 3B can further validate the above suggestion. As can be seen, PAg-TiO_2 does not obviously enhance the photogenerated charge lifetime of TiO_2, while the charge lifetimes for SAg-TiO_2(5 nm), and SAg-TiO_2(1 nm) are 34% and 93% increment (from 4.79 ns to 6.44 ns and 9.26 ns), respectively. It indicates that an appropriate size of the loaded Ag NPs is beneficial for improving the carrier separation, and resulting in a much longer charge lifetime. From the above results and discussions on the DRS, PL and the time-resolved PL spectra, it can be concluded that the ultrafine SAg NPs can greatly affect the photogenerated electron-hole separation, and then prolong the carrier lifetime, which is beneficial for improving the photoactivity.

Photocatalytic activities of PAg-TiO_2 and SAg-TiO_2 were evaluated in terms of the degradation of rhodamine B (RhB, 10 mg L^{-1}) under visible light ($\lambda \geq 420$ nm) irradiation as shown in Fig. 4A. As can be seen, the pristine TiO_2 and PAg-TiO_2(20 nm) only display limited visible-light-driven photocatalytic degradation (PCD) rate of RhB, while the PCD reaction rate constants are 3.2, 1.16, 0.32, 0.15 h^{-1} for SAg-TiO_2(1nm), SAg-TiO_2(5nm), PAg-TiO_2(20 nm) and TiO_2, respectively. Namely, SAg-TiO_2(1 nm) exhibits the best photoactivity under the visible-light irradiation. Usually, the photocatalytic performance might influenced by many factors such as the light absorption intensity, carrier lifetime, crystalline and size, etc, and the PCD results may come from a synergistic effect of several factors. However, Ag NPs size is the most key factor contributing to the photoactivity based on the present research results. On one hand, all SAg-TiO_2 samples with small Ag size show much better visible light absorption than PAg-TiO_2 and TiO_2 as observed from the DRS spectra in Fig. 2. On the other hand, the smaller Ag NPs of SAg-TiO_2 can easily to promote the photogenerated carrier separation, which obviously prolongs the carrier lifetime as mentioned above. Therefore, it is reasonable to observe the higher photoactivity of SAg-TiO_2 than PAg-TiO_2 and pure TiO_2 for the degradation of RhB under visible light irradiation.

Furthermore, SAg-TiO_2 (1 nm) with 1 nm Ag NPs on TiO_2 facets derived from the present in situ photoreduction process exhibits substantial photoactivity and stability under visible light irradiation as shown in Fig. S4. The photoactivity after 10 cycles did not display a significant decrease. To further understand the involvement of active radical species in the photocatalytic process, control experiments with adding scavenger for h^+, $^{\bullet}O_2^-$ and $^{\bullet}OH$ have been carried out, and the corresponding results are shown in Fig. 5A. The PCD reaction rate of RhB over SAg-TiO_2 (1 nm) was remarkably decreased when triethanolamine (TEOA) as a hole-scavenger or isopropanol as a hydroxyl radicals ($^{\bullet}OH$) scavenger is added into the photoreaction system; while p-benzoquinone (BQ) as a quencher of $^{\bullet}O_2^-$ only shows minimal impact on the RhB PCD reaction rate. Therefore, it can be concluded that •OH and h^+ are the main active species in photocatalytic process of SAg-TiO_2 (1 nm) aqueous suspension under visible light irradiation. Similarly, PAg-TiO_2(20 nm) suspension also shows the same change trends in the photoactivity as SAg-TiO_2(Fig. 5B) after the addition of the above active radical species. The above results indicate the photocatalytic activity is mainly related to Ag NPs size loaded of TiO_2 facets, which played an important role on surface plasmon resonance (SPR) effect and the photogenerated carrier separation process. Moreover, those Ag NPs loaded on TiO_2 facets shows size-dependent photoactivity, highly suggesting that there is still a wide scope to tailor the photoactivity of noble

metal NPs loaded semiconductor by tuning the metal particle sizes in the present in situ photoreduce approach.

Conclusions

In summary, anatase TiO_2 nanocrystals with regular polyhedron morphology and co-exposed {001} and {101} facets are prepared, and then SAg-TiO_2 with ultrafine Ag NPs uniformly dispersed on the TiO_2 facets have been successfully synthesized by a novel in situ photoreduction approach, the minimal size (1 nm) of Ag NPs can be loaded on both {001} and {101} facets of TiO_2 under an optimal UV wavelength and reaction temperature. Such SAg-TiO_2 with much smaller Ag NPs and high dispersity on both {001} and {101} facets shows excellent visible-light-responsive photocatalytic activity and stability, far exceeding that of PAg-TiO_2 with much larger Ag NPs size (20 nm) only loaded on {001} facets of TiO_2. Moreover, those Ag NPs loaded on TiO_2 facets shows size-dependent photoactivity, and smaller Ag NPs can not only enhance the SPR effect, but also act as a more advanced media to promote the photogenerated carrier separation. The present work clearly reveals that the particle size of precious metal NPs loaded on semiconductor is one of the most key factors contributing to the photoactivity. It is hoped that this work could render guided information for the other M@semiconductor (M = Au, Pt, Cu, Pd) nanostructured materials with tunable photocatalytic activity.

Acknowledgements

This work was supported by the National Natural Science Foundation of China (21273164, 21271146, and 20973128), the Funds for Creative Research Groups of Hubei Province (2014CFA007), the open foundation of Key Laboratory of Catalysis and Materials Science, South-Central University for Nationalities, the Fundamental Research Funds for the Central Universities (2042014kf0228) and the Large-scale Instrument Equipment Sharing Foundation of Wuhan University.

References

1 H. G. Yang, C. H. Sun, S. Z. Qiao, J. Zou, G. Liu, S. C. Smith, H. M. Cheng and G. Q. Lu, *Nature*, 2008, **453**, 638–641.

2 H. G. Yang, G. Liu, S. Z. Qiao, C. H. Sun, Y. G. Jin, S. C. Smith, J. Zou, H. M. Cheng and G. Q. Lu, *J. Am. Chem. Soc.*, 2009, **131**, 4078–4083.

3 Ni, M.; Leung, M. K. H.; Leung, D. Y. C.; Sumathy, K. *Renew Sust Energ Rev.* 2007, **11**, 401–425.

4 M. R. Hoffmann, S. T. Martin, W. Choi, D. W. Bahnemann, *Chem. Rev.* 1995, **95**, 69–96.

5 Schmidt, C. M.; Buchbinder, A. M.; Weitz, E.; Geiger, F. M. *J. Phys. Chem. A* 2007, **111**, 13023–13031.

6 R. G. Li, F. X. Zhang, D. G. Wang, J. X. Yang, M. R. Li, J. Zhu, X. Zhou, H. X Han, C. Li. *Nat. Commun*. **4**:1432 (2013).

7 L. Q. Liu, S. X. Ouyang, J. H. Ye, *Angew. Chem. Int. Ed.* 2013, **52**, 1–6

8 K. Cheng, W. B. Sun, H. Y. Jiang, J. J. Liu, J. Lin, *J. Phys. Chem. C* 2013, **117**, 14600−14607

9 S. Y. Zhu, S. J. Liang, Q. Gu, L. Y. Xie, J. X. Wang, Z. X. Ding, P. Liu, *Appl. Catalysis B: Environ.* **119–120** (2012) 146–155

10 Choi, W.; Termin, A.; Hoffmann, M. R. *J. Phys. Chem.* 1994, **98**, 13669–13679.

11 Takeuchi, M.; Yamashita, H.; Matsuoka, M.; Anpo, M.; Hirao, T.; Itoh, N. N. *Catal. Lett.* 2000, **67**, 135–137.

12 Asahi, R.; Morikawa, T.; Ohwaki, T.; Aoki, K.; Taga, Y. *Science* 2001, **293**, 269–271.

13 Khan, S. U. M.; Al-Shahry, M.; Ingler, W. B. *Science* 2002, **297**, 2243–2245.

14 J. X. He, P. J. Yang, H. Sato, Y. Umemura, A. Yamagishi, *J Electroanal Chem* **566** (2004) 227–233

15 M. V. Sofianou, N. Boukos, T. Vaimakis, C. Trapalis, *Appl. Catalysis B: Environ.* **158–159** (2014) 91–95

16 X. F. You, F. Chen, J. L. Zhang, M. Anpo, *Catal Lett.* **102**, 3–4, August 2005.

17 R.M. Mohamed, I.A. Mkhalid, *J. Alloys Compd.* **501** (2010) 301–306.

18 S.X. Liu, Z.P. Qu, X.W. Han, C.L. Sun, *Catal Today* **93–95** (2004) 877–884

19 X. G. Han, Q. Kuang, M. S. Jin, Z. X. Xie, L. S. Zheng. *J.Am. Chem. Soc.* 2009, **131**, 3152-3153.

20 L. Q. Ye, J. Mao, J. Y. Liu, Z. Jiang, T. Y. Peng, L. Zan, *J. Mater. Chem.* A, 2013, 1: 10532–10537.

21 Read, C. G., Steinmiller, E. M. P. & Choi, K. S. et al. *J. Am. Chem. Soc.* **131**, 12040–12041 (2009).

22 Miseki, Y., Kato, H. & Kudo, A. et al. *Energy Environ. Sci.* **2**, 306–314 (2009).

23 E. Stathatos, P. Lianos, *Langmuir* **16** (2000) 2398.

24 D. M. Schaadt, B. Feng, and E. T. Yu, *Appl Phys Lett* **86**, 063106 (2005);

25 T. R. Jensen, M. D. Malinsky, C. L. Haynes, R. P. Van Duyne, *J. Phys. Chem. B* 2000, **104**, 10549-10556

26 J.C. Yu, J.G. Yu, W.K. Ho, Z.T. Jiang, L.Z. Zhang, *Chem. Mater*. **14** (2002) 3808.

27 F.B. Li, X.Z. Li, *Chemosphere* **48** (2002) 1103.

28 L. Q. Ye, K. J. Deng, F. Xu, L. H. Tian, T. Y. Peng, L. Zan, *Phys. Chem. Chem. Phys.*, 2012, **14**, 82–85.

29 Henglein, A.; Meisel, D. *Langmuir* 1998, **14**, 7392.

30 Henglein, A. *Langmuir* 1999, **15**, 6738

31 P. V. Kamat, *J. Phys. Chem. B* 2002**, 106**, 7729-7744.

32 W. N. Wang, W. J. An, B. Ramalingam, S. Mukherjee, D. M. Niedzwiedzki, S. Gangopadhyay, P. Biswas, *J. Am. Chem. Soc*. 2012, **134**, 11276−11281.

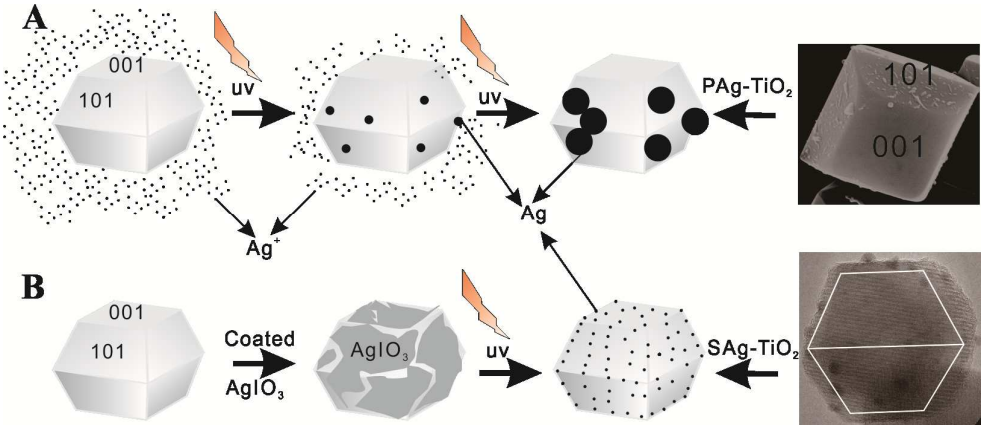

Scheme 1 The proposed growth mechanism of Ag NPs during PAg-TiO_2(A) and SAg-TiO_2(B) preparation processes.

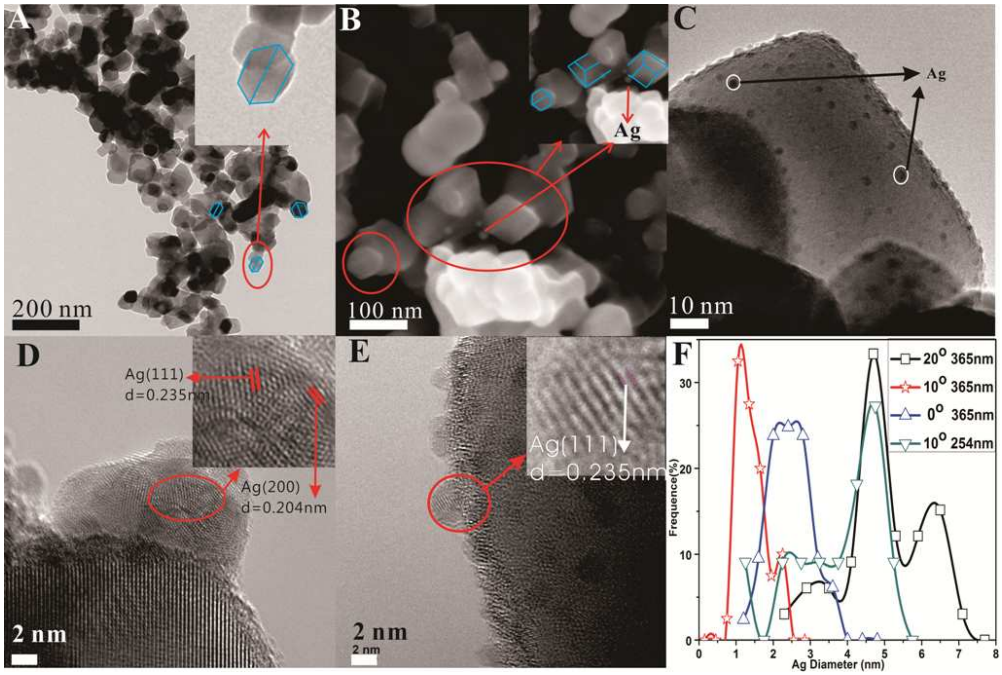

Fig. 1 (A) TEM image of TiO_2 nanocrystals with co-exposed facets; (B) SEM image of PAg-TiO_2; (C) TEM image of SAg-TiO_2 synthesized at 10°C and 365 nm UV light irradiation; (D) HRTEM image of PAg-TiO_2; (E) HRTEM image of SAg-TiO_2 (1 nm); (F) Size distribution of Ag NPs on anatase TiO_2 derived from TEM images shown in Fig. S1.

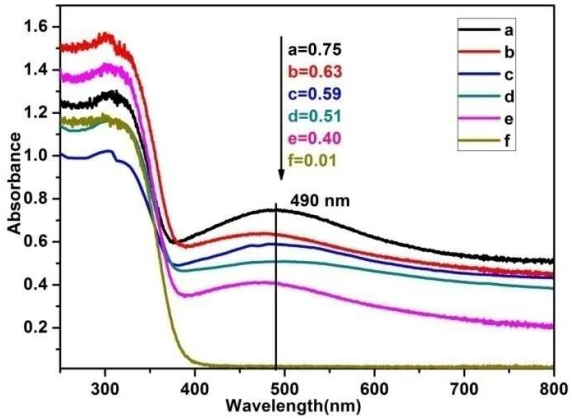

Fig. 2 UV–Vis diffuses reflectance spectra (DRS) of the samples. a) SAg-TiO_2(1 nm); b) SAg-TiO_2(2.4 nm); c) SAg-TiO_2(5 nm); d) SAg-TiO_2(6 nm); e) PAg-TiO_2(20 nm); f) TiO_2.

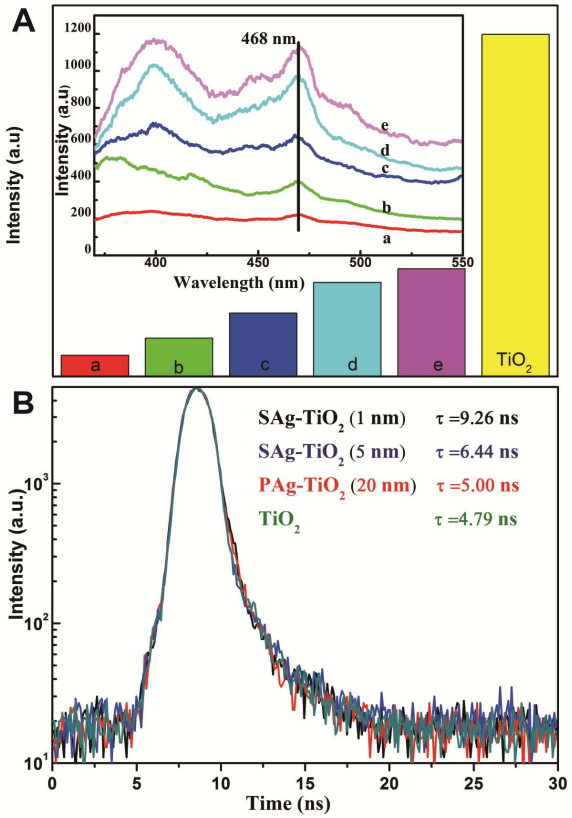

Fig. 3 (A) Photoluminescence (PL) spectra of PAg-TiO_2, SAg-TiO_2 and TiO_2. a) SAg-TiO_2 (1 nm); b) SAg-TiO_2 (2.4 nm); c) SAg-TiO_2 (5 nm); d) SAg-TiO_2 (6 nm); e) PAg-TiO_2 (20 nm); f) TiO_2; (B) time-resolved PL spectra of the above samples.

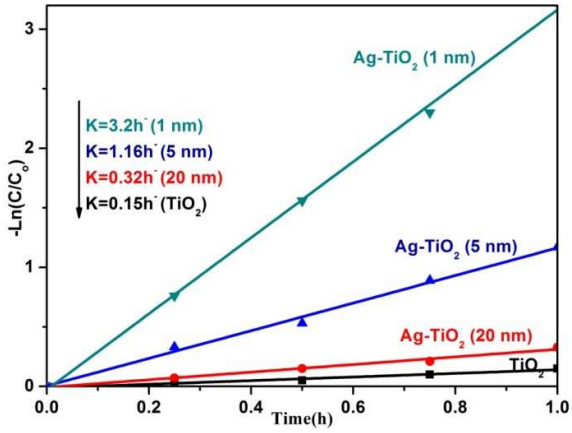

Fig. 4 Pseudo first-order reaction kinetics of the RhB photodegrdation reaction of SAg-TiO_2(1 nm), SAg-TiO_2(5 nm), PAg-TiO_2(20 nm), and TiO_2.

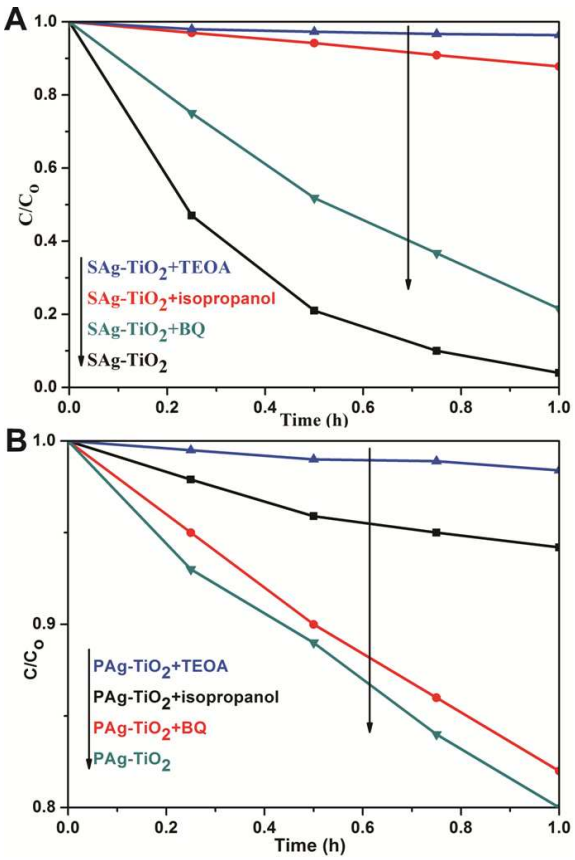

Fig. 5 Plots of the photogenerated active species trapping in the system of photodegradation of RhB under visible light irradiation over the samples, (A) SAg-TiO_2(1 nm); (B) PAg-TiO_2(20 nm).

TOC

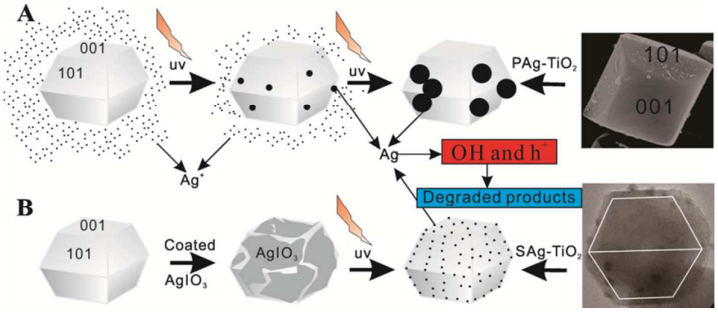

The proposed growth mechanism of Ag NPs during PAg-TiO_2(A) and SAg-TiO_2(B) preparation processes.